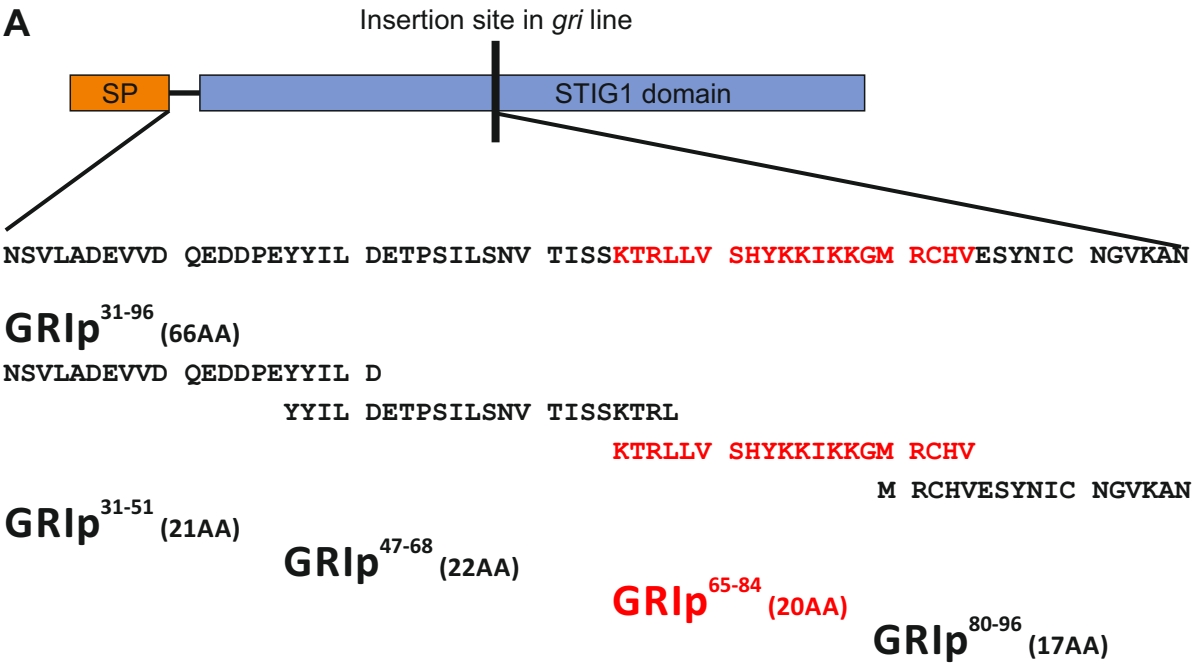

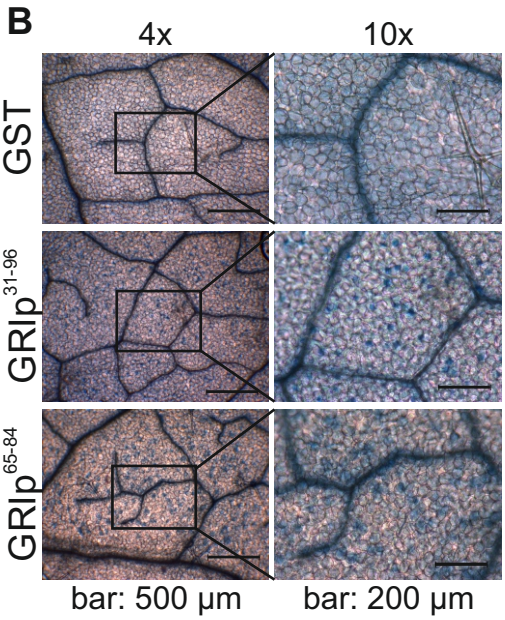

Fig. S1. A 20 aa peptide derived from GRI is sufficient to induce cell death in *Arabidopsis* leaves.

A Schematic representation of GRI protein and GRI-peptides. Sequences of GRIp$^{31-96}$, GRIp$^{31-51}$, GRIp$^{47-68}$, GRIp$^{65-84}$ and GRIp$^{80-96}$ are shown underneath.

B Col-0 leaves were infiltrated with 37 nM GST, GRIp$^{31-96}$ or GRIp$^{65-84}$ and subsequently stained with Trypan blue. Pictures were taken under a light microscope at 4x and 10x magnification, respectively.

Data information: The experiment has been repeated six times with similar results.

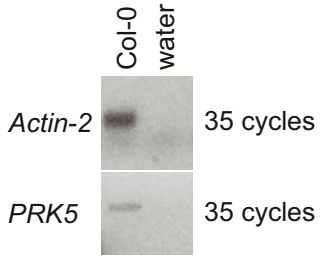

Fig. S2. *PRK5* transcript is present in low levels in the leaves of wild type *Arabidopsis* Col-0 plants.

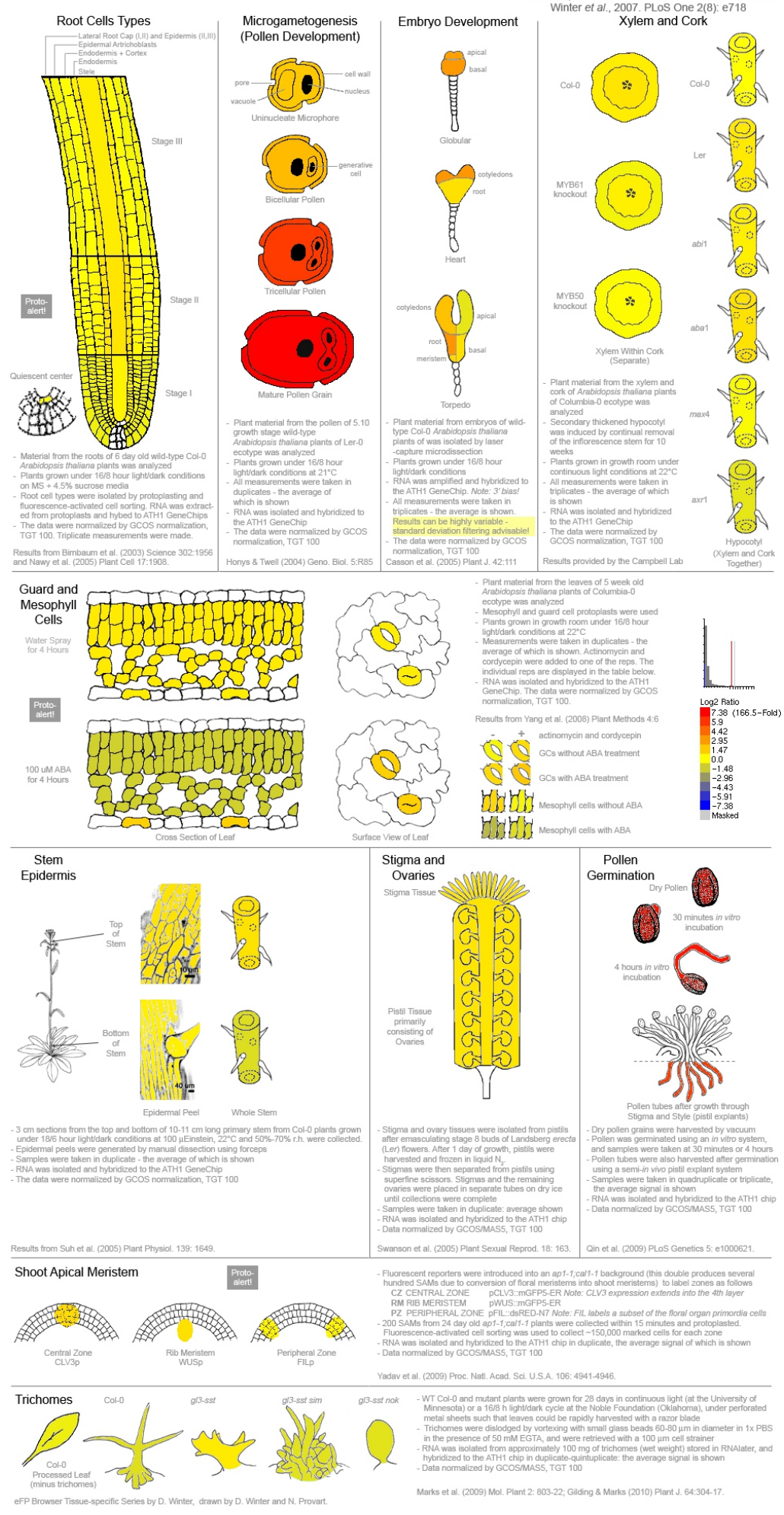

Fig. S3. Expression of *PRK5* transcript *Arabidopsis* tissues (eFP browser, developmental map; http://bar.utoronto.ca/efp/cgi-bin/efpWeb.cgi).

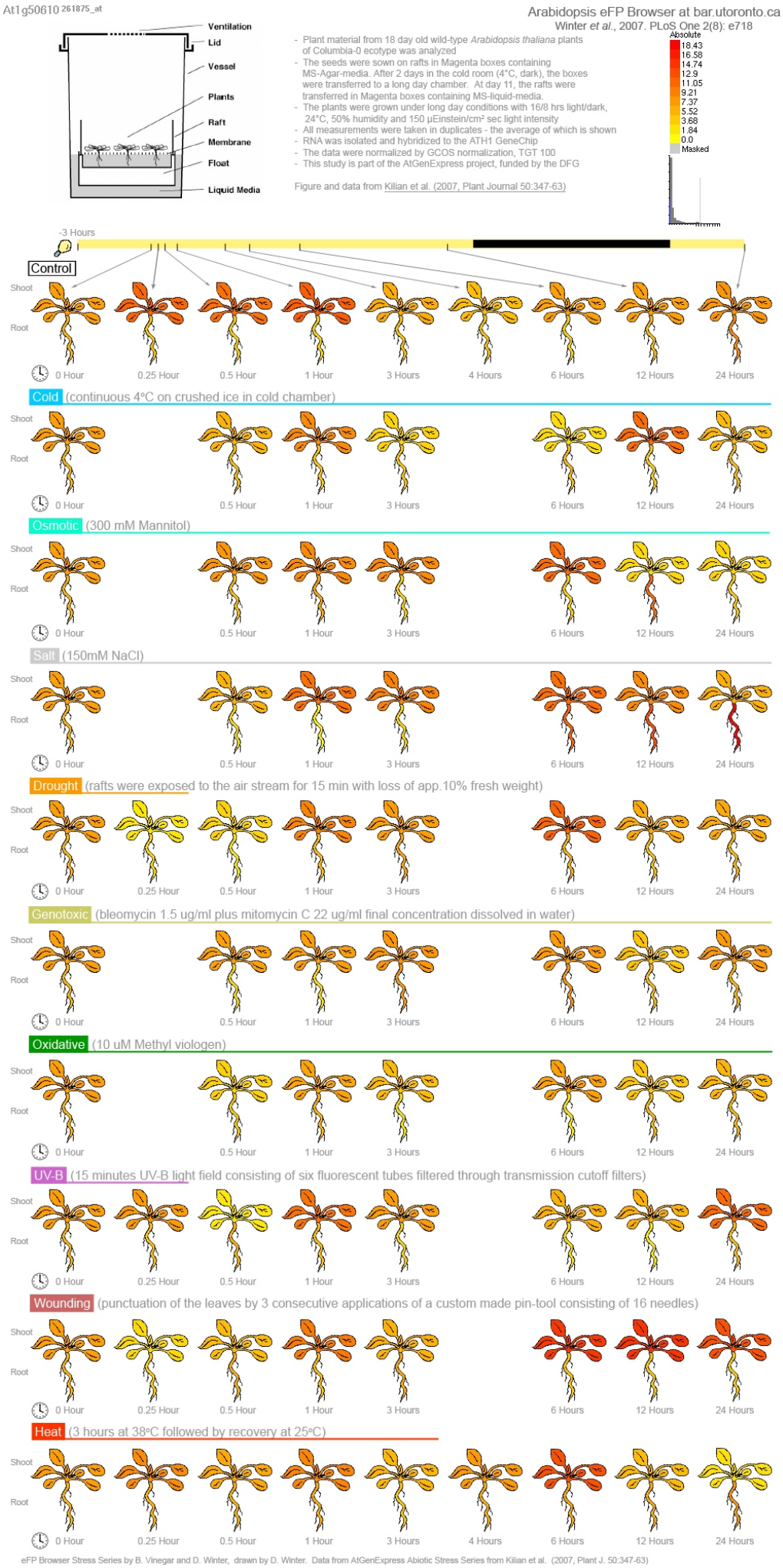

Fig. S4. *PRK5* transcript levels are altered in response to a variety of abiotic stresses in *Arabidopsis* (eFP browser, Abiotic stress I; http://bar.utoronto.ca/efp/cgi-bin/efpWeb.cgi).

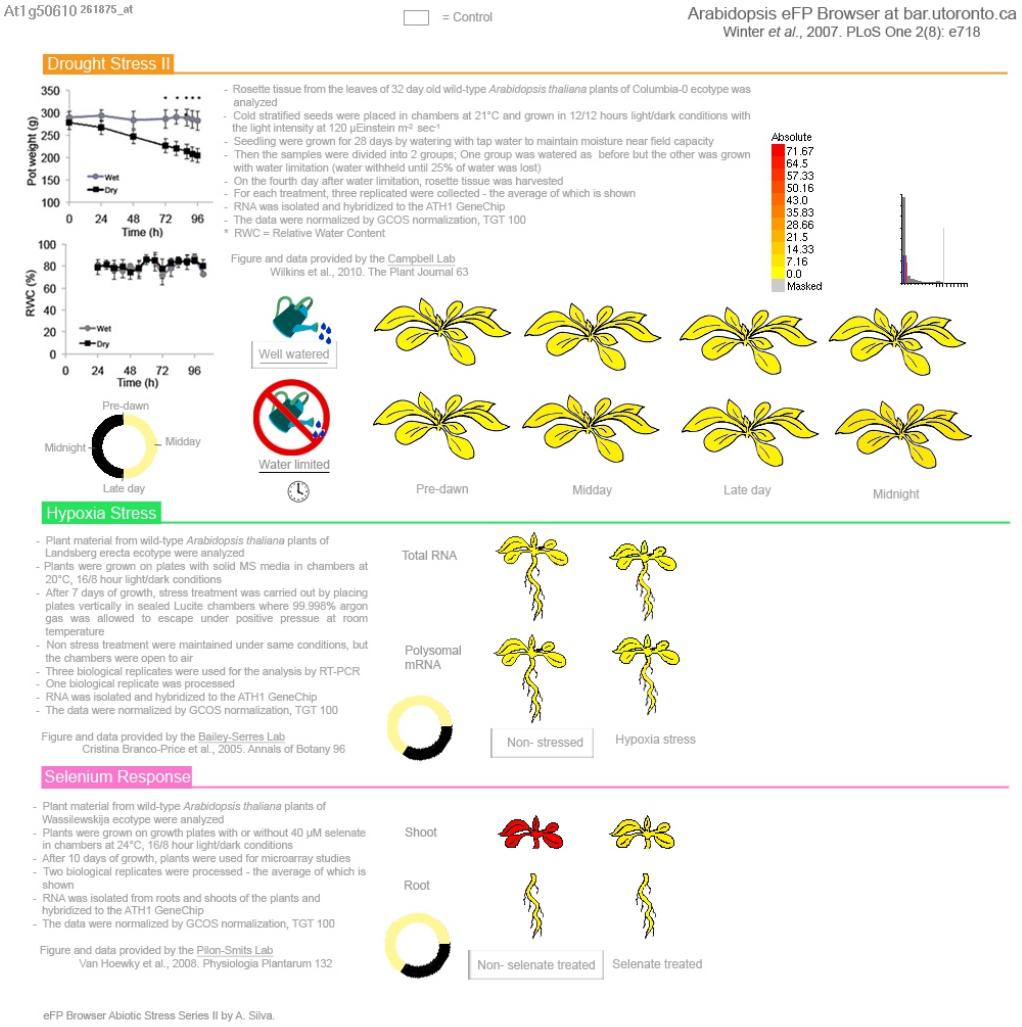

Fig. S5. *PRK5* transcript levels are altered in response to a variety of abiotic stresses in *Arabidopsis* (eFP browser, Abiotic stress II; http://bar.utoronto.ca/efp/cgi-bin/efpWeb.cgi).

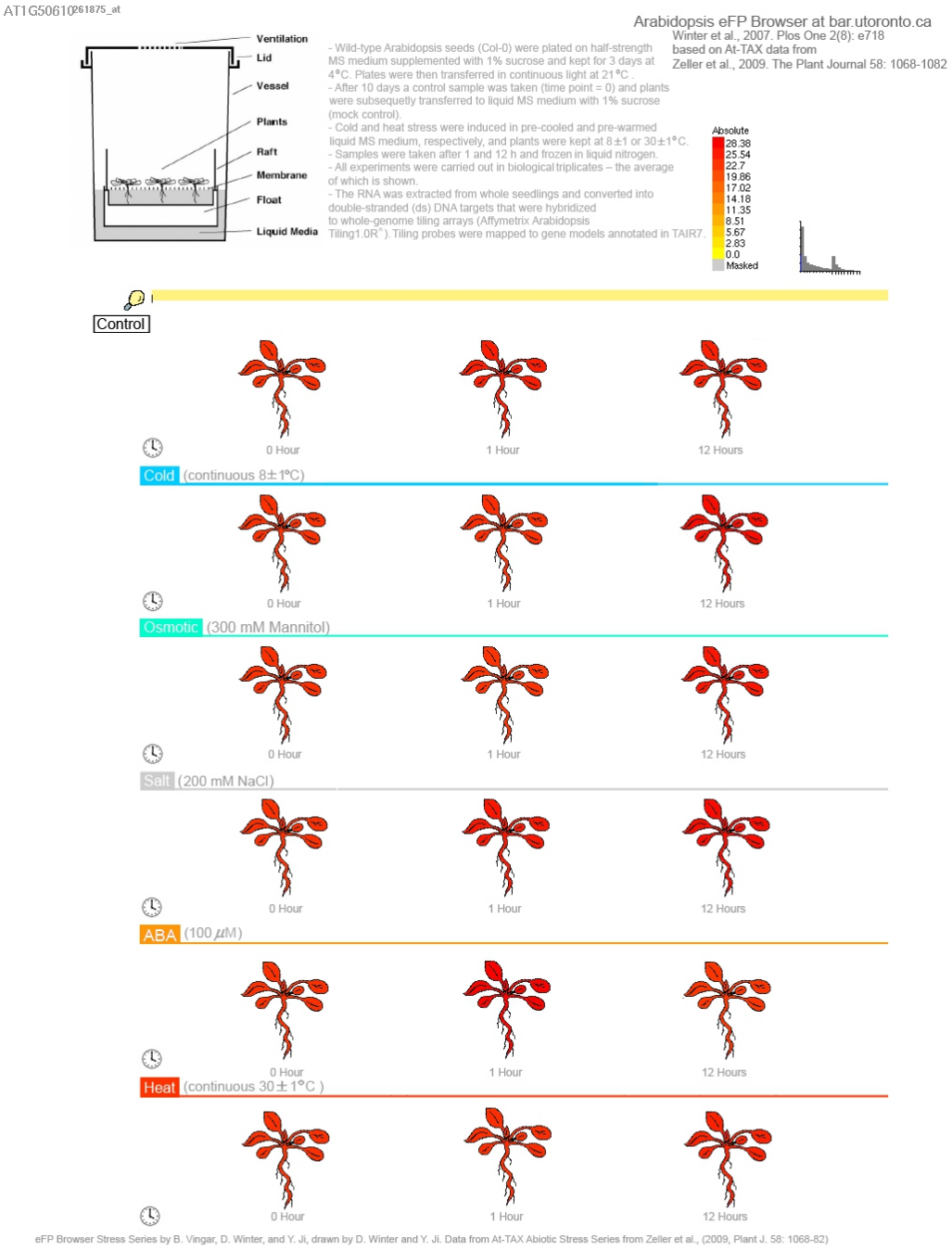

Fig. S6. *PRK5* transcript levels are altered in response to a variety of abiotic stresses in *Arabidopsis* (eFP browser, Abiotic stress At-TAX; http://bar.utoronto.ca/efp/cgi-bin/efpWeb.cgi).

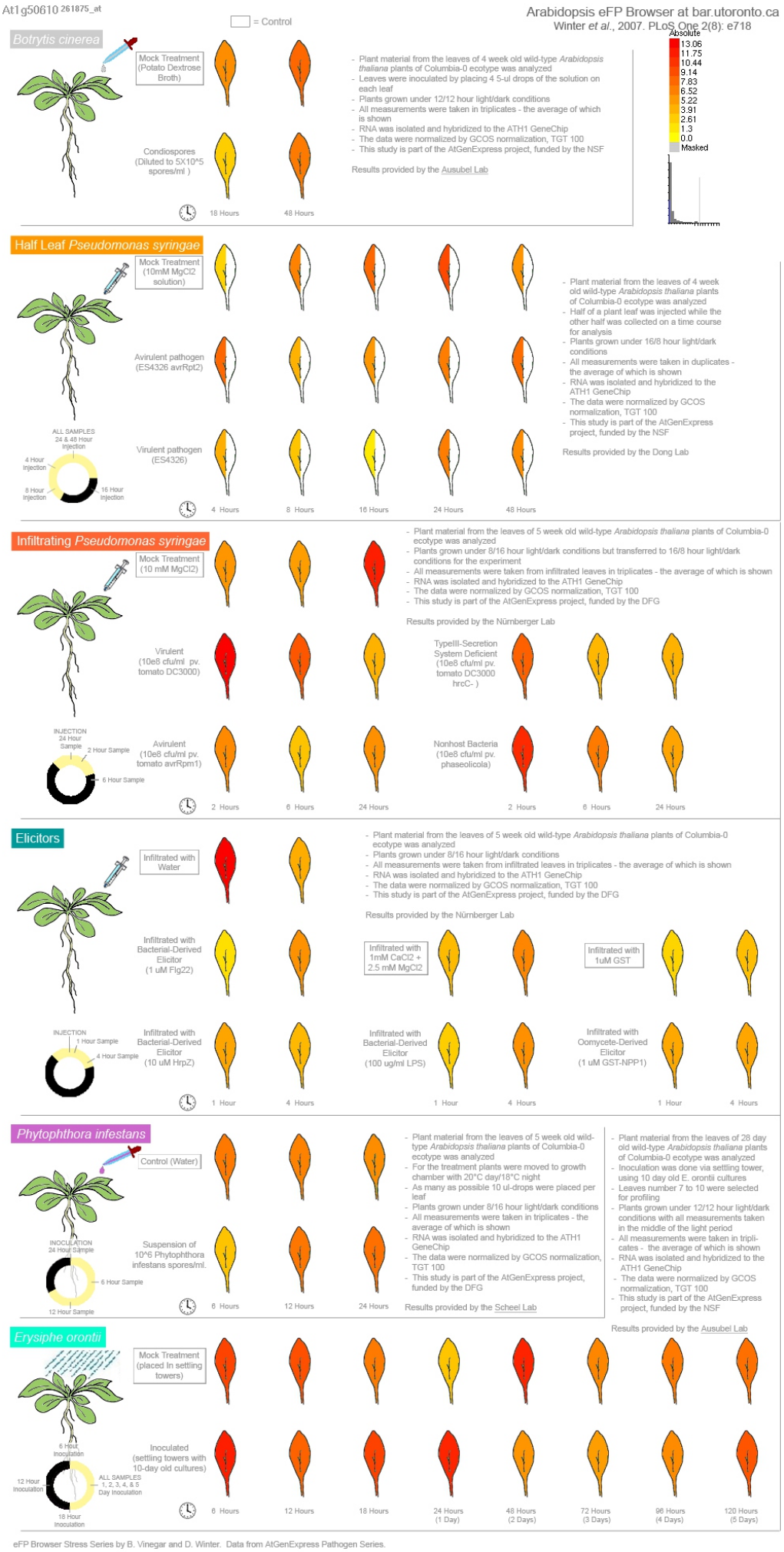

Fig. S7. *PRK5* transcript levels are altered in response to pathogen infection in *Arabidopsis* (eFP browser, Biotic stress I; http://bar.utoronto.ca/efp/cgi-bin/efpWeb.cgi).

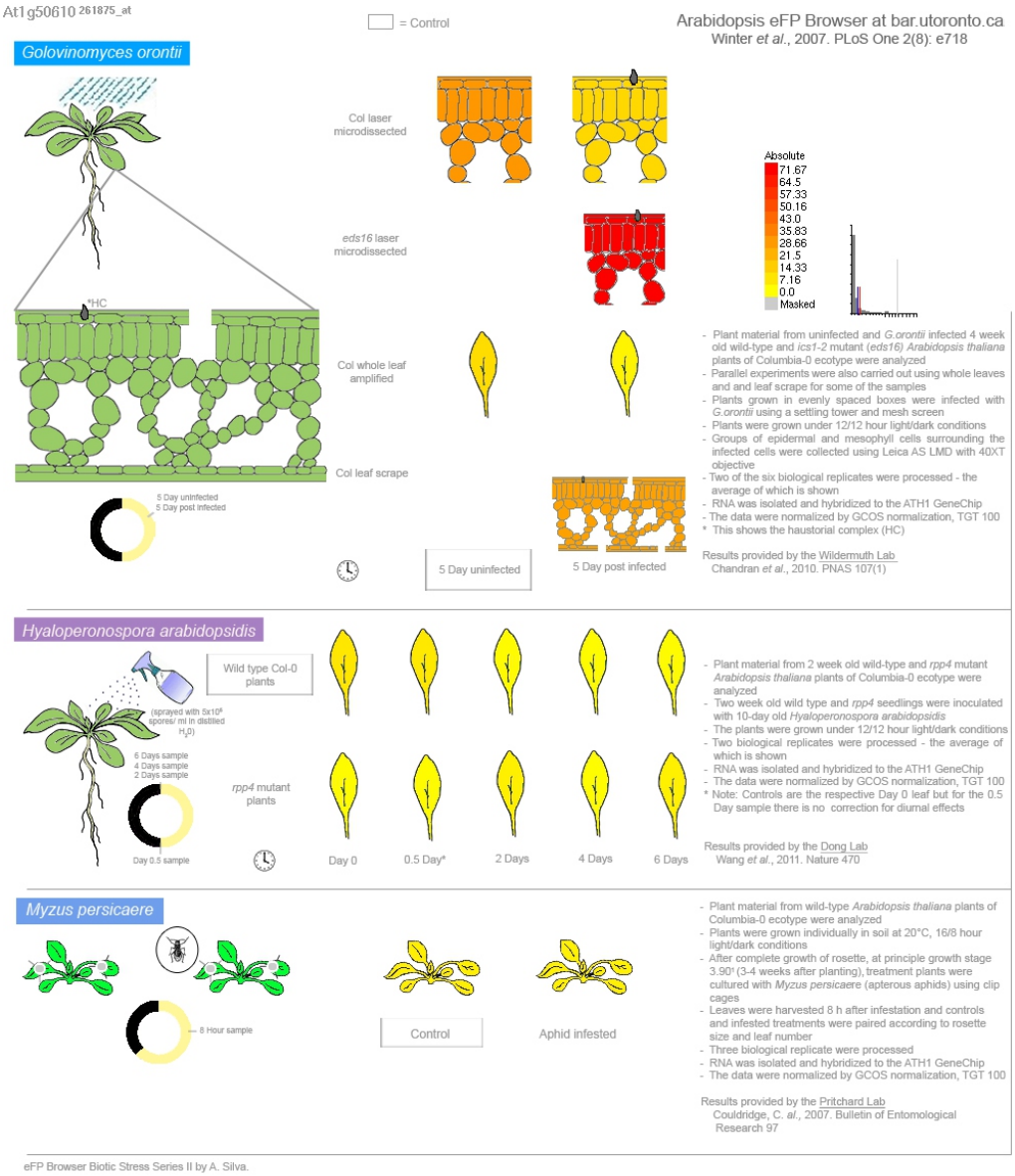

Fig. S8. *PRK5* transcript levels are altered in response to pathogen infection in *Arabidopsis* (eFP browser, Biotic stress II; http://bar.utoronto.ca/efp/cgi-bin/efpWeb.cgi).

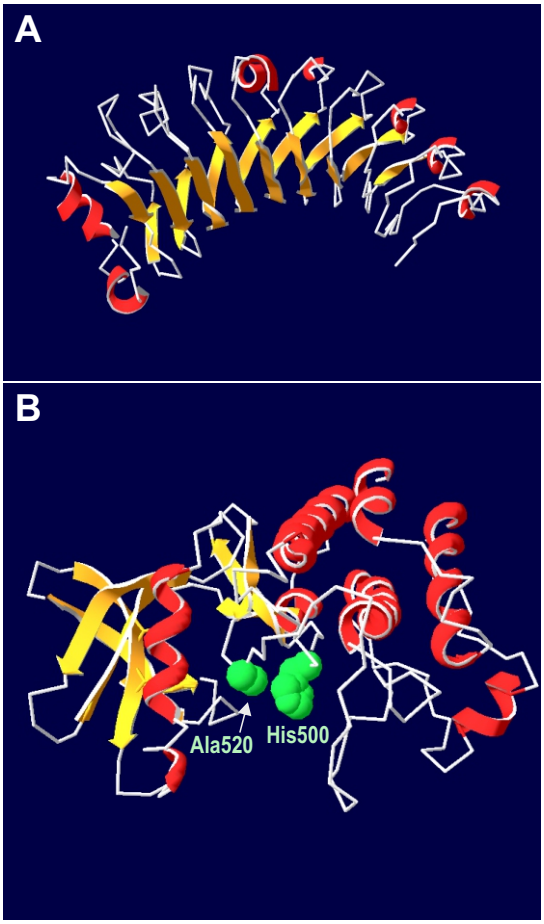

Fig. S9. Structural prediction of PRK5 extracellular and intracellular domains.

A I-Tasser prediction of the extracellular domain of PRK5 (residues 40-281).

B Phyre[2] prediction of the intracellular kinase domain of PRK5 (residues 375-645). Histidine residue 500 and alanine residue 520 are shown in green.

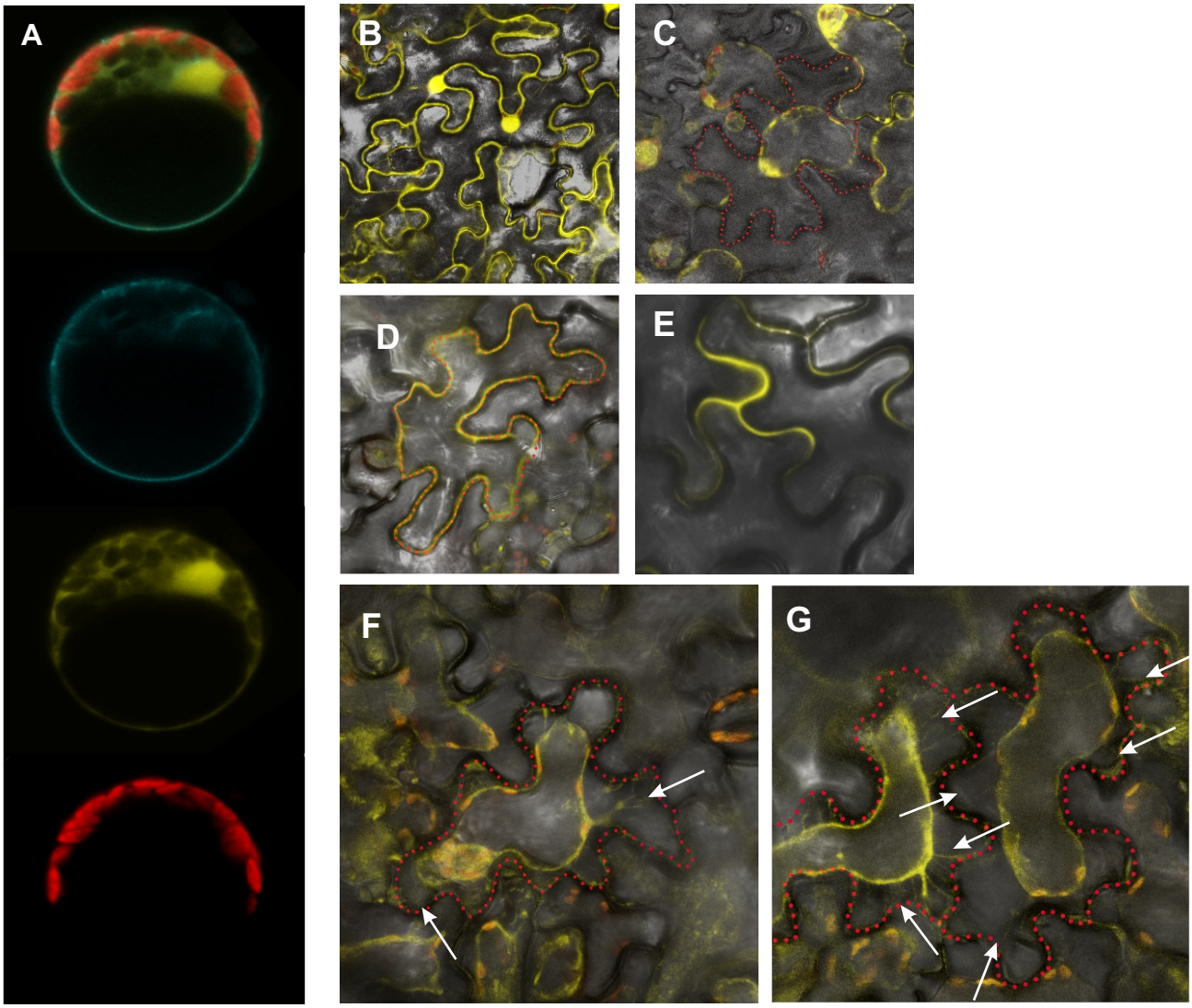

Fig. S10. PRK5-YFP localises to the plasma membrane in *Arabidopsis* protoplasts and in *Nicotiana benthamiana*.

A Localization of PRK5-CFP and cytosolic YFP in Col-0 mesophyll protoplasts. Panels from top to bottom: overlay, PRK5-CFP, YFP, chloroplast.

B YFP (expressed under the control of the 35S promoter) localises to the cytosol and nucleus in epidermal cells of *Nicotiana benthamiana*.

C After plasmolysis with 0.8 M NaCl for 15 minutes YFP is visible in the cytosol and nucleus *in Nicotiana benthamiana* epidermal cells.

D, E PRK5-YFP (expressed under the control of the 35S promoter) localises to the plasma membrane in *Nicotiana benthamiana* epidermal cells.

F, G After plasmolysis with 0.8 M NaCl for 15 minutes PRK5-YFP is visible in the plasma membrane in *Nicotiana benthamiana* epidermal cells as indicated by the appearance of Hechtian strands (see arrow heads).

Data information: Experiments in this figure have been repeated three times with similar results.

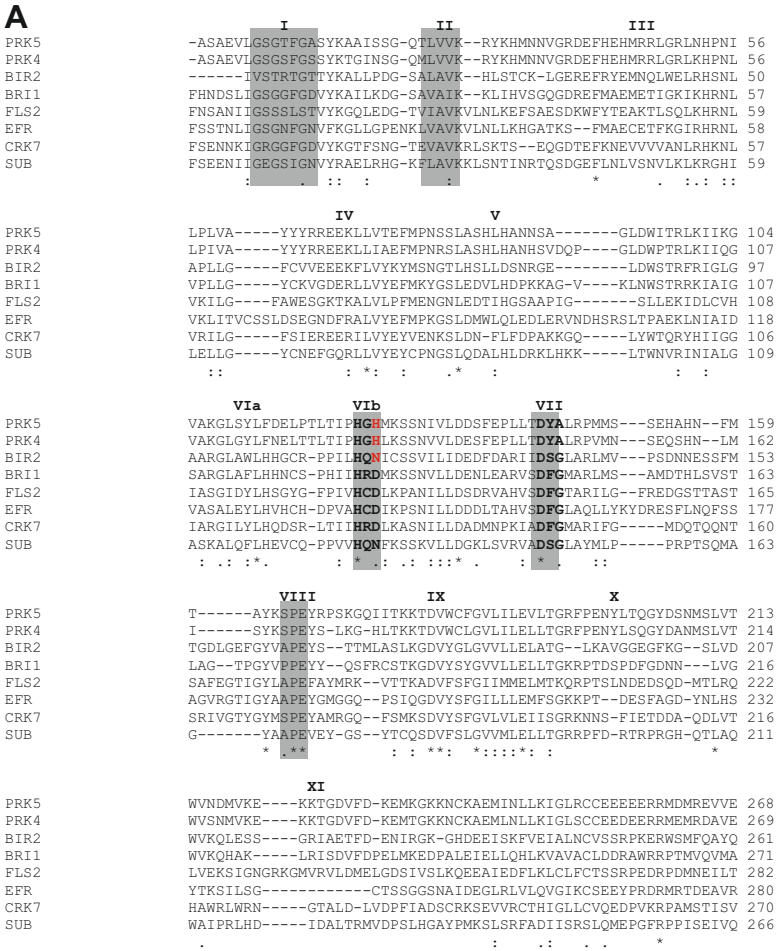

Fig. S11. Conservation of the kinase domain and *in vitro* kinase activity of PRK5 and PRK5$^{H500D\ A520G}$ kinase domains.

A Alignment of kinase domains of the inactive kinases PRK4, PRK5, BIR2 as well as SUB with the active kinase domains of BRI1, FLS2, EFR and CRK7.

B Phyre2 prediction of the catalytic core of the intracellular kinase domain of PRK5. Histidine (H) at position 500 and alanine (A) at position 520 are shown in green.

C Phyre2 prediction of the intracellular kinase domain of PRK5; introduced mutations H500D and A520G. D and G in the catalytic core are highlighted in green.

D *In vitro* phosphorylation assays of GST-PRK5 kinase domain in the presence of 10 mM $MgCl_2$. GST-PRK5 and GST-PRK4 did not show kinase activity while mutation of H500D and A520G restored GST-PRK5$^{H500D\ A520G}$ kinase activity. GST-CRK7 was used as a positive control. Upper panel shows autoradiograph, lower panel shows the Coomassie-stained 15% SDS-polyacrylamide gel. Arrows indicate the GST-tagged RLK kinase domains, the size of free GST and myelin basic protein (MBP; used as artificial substrate).

Data information: Experiments have been repeated three times with similar results.

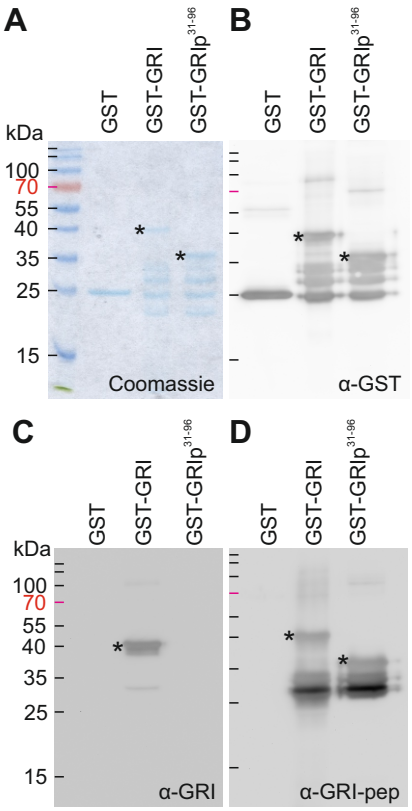

Fig. S12. Western blot of GST, GST-GRI and GST-GRIp$^{31-96}$.

A Coomassie brilliant blue stained polyacrylamide gel of bacterially produced GST, GST-GRI (asterisk) and GST-GRIp$^{31-96}$ (asterisk).

B Western blot of bacterially produced GST, GST-GRI (asterisk) and GST-GRIp$^{31-96}$ (asterisk) with α-GST antibody.

C Western blot of bacterially produced GST, GST-GRI (asterisk) and GST-GRIp$^{31-96}$ with α-GRI antibody.

D Western blot of bacterially produced GST, GST-GRI (asterisk) and GST-GRIp$^{31-96}$ (asterisk) with α-GRI-pep antibody.

E Sequence alignment of PRK5 and PRK4 protein sequences.

F Interaction of GST-GRI and GST-GRIp$^{31-96}$ with the ectodomain of FLS2. GST-GRIp$^{31-96}$ showed stronges interaction with the ectodomain of PRK5 and weak interaction with PRK4. No interaction was detected with the ectodomain of FLS2.

E

```
PRK5  MRNWEDPFTLACNTALKKNLPSCIFIIIFISVLCPVAMSQ-----VVVPDSDADCLLRFK 55
PRK4  MLTWETPVMLASNTASTKKLAFITTFLIIVLCPVTMVMSQPQADVLPLPASDADCLLRFK 60
      * .** *. **.*** .*:*.    ::*::    .:.***     : :* **********

PRK5  DTLANGSEFRSWDPLSSPCQGNTANWFGVLCSN-YVWGLQLEGMGLTGKLNLDPLVPMKN 114
PRK4  DTLVNASFISSWDPSISPCKRNSENWFGVLCVTGNVWGLQLEGMGLTGKLDLEPLAAIKN 120
      ***.*.* : ****  ***: *: ******* .  ***************:*:**..:**

PRK5  LRTISFMNNNFNGPMPQVKRFTSLKSLYLSNNRFSGEIPADAFLGMPLLKKILLANNAFR 174
PRK4  LRTLSFMNNKFNGSMPSVKNFGALKSLYLSNNRFTGEIPADAFDGMHHLKKLLLANNAFR 180
      ***:*****:***.**.**.* :************:******** **  ***:********

PRK5  GTIPSSLASLPMLLELRLNGNQFQGQIPSFQQKDLKLASFENNDLDGPIPESLRNMDPGS 234
PRK4  GSIPSSLAYLPMLLELRLNGNQFHGEIPYFKQKDLKLASFENNDLEGPIPESLSNMDPVS 240
      *:****** ***************:*:** *:***************:******* **** *

PRK5  FAGNKGLCDAPLSPCSSSSPGVPVVPVSPVDPKSTSPPTGKKAGSFYTLAIILIVIGIIL 294
PRK4  FSGNKNLCGPPLSPCSSDSGSSPDLPSSPTEKN--------KNQSFFIIAIVLIVIGIIL 292
      *:***.**..*******.* . * :* **.: :        *  **: :**:********

PRK5  VIIALVFCFVQSRRRNFLSAYPSSAGKERIESYNYHQSTNKNNKPAESVN--HTRRGSMP 352
PRK4  MIISLVVCILHTRRRKSLSAYP-SAGQDRTEKYNYDQSTDKD-KAADSVTSYTSRRGAVP 350
      :**:**.*::::***: ***** ***::* *.***.***:*: *.*:**.   :***::*

PRK5  DPGGRLLFVRDDIQRFDLQDLLRASAEVLGSGTFGASYKAAISSGQTLVVKRYKHMNNVG 412
PRK4  DQN-KLLFLQDDIQRFDLQDLLRASAEVLGSGSFGSSYKTGINSGQMLVVKRYKHMNNVG 409
      * . :***::**********************:**:***:.*.*** **************

PRK5  RDEFHEHMRRLGRLNHPNILPLVAYYYRREEKLLVTEFMPNSSLASHLHANNSA---GLD 469
PRK4  RDEFHEHMRRLGRLKHPNLLPIVAYYYRREEKLLIAEFMPNRSLASHLHANHSVDQPGLD 469
      **************:***:**:************::***** *********:*.   ***

PRK5  WITRLKIIKGVAKGLSYLFDELPTLTIPHGHMKSSNIVLDDSFEPLLTDYALRPMMSSEH 529
PRK4  WPTRLKIIQGVAKGLGYLFNELTTLTIPHGHLKSSNVVLDESFEPLLTDYALRPVMNSEQ 529
      * ******:******.***:**.********:****:***:**************:*.**:

PRK5  AHNFMTAYKSPEYRPSKGQIITKKTDVWCFGVLILEVLTGRFPENYLTQGYDSNMSLVTW 589
PRK4  SHNLMISYKSPEYS-LKG-HLTKKTDVWCLGVLILELLTGRFPENYLSQGYDANMSLVTW 587
      :**:* :******   **  :********:******:**********:****:*******

PRK5  VNDMVKEKKTGDVFDKEMKGKKNCKAEMINLLKIGLRCCEEEEERRMDMREVVEMVEMLR 649
PRK4  VSNMVKEKKTGDVFDKEMTGKKNCKAEMLNLLKIGLSCCEEDEERRMEMRDAVEKIERLK 647
      *.:***************.*********:******* ****:*****:**:.** :* *:

PRK5  EGESEDDFGSMDHRGTHNNVYSSMLLDDDDFGFSMNR 686
PRK4  EGEFDNDFASTTH-----NVFASRLIDDDDFGFAMNR 679
      *** ::**.*  *     **::* *:********:***
```

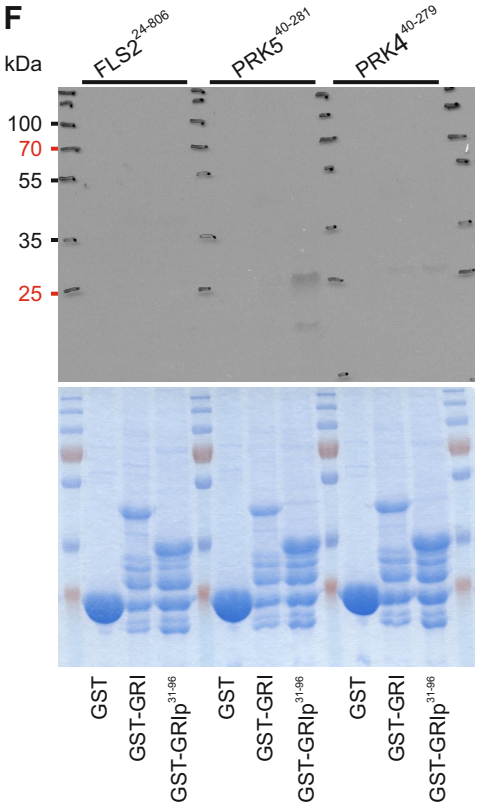

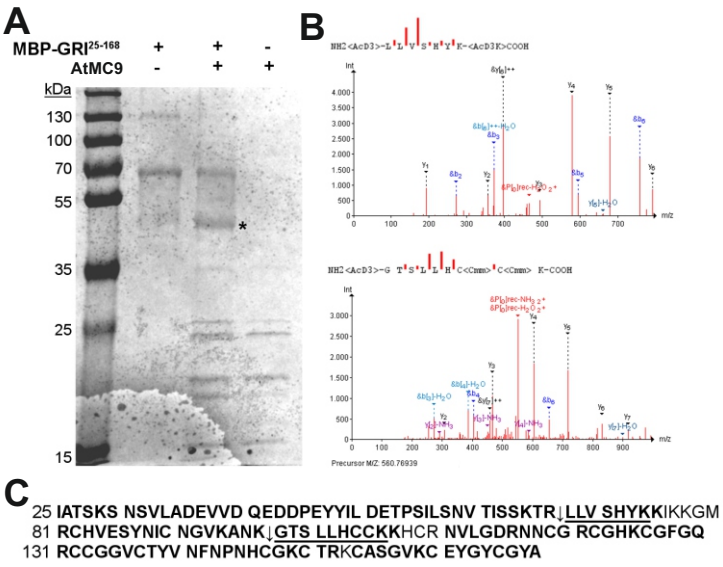

Fig. S13. GRI is cleaved by AtMC9 after K65, R67, K78 and K97, as revealed by *in vitro* cleavage assays and mass spectrometry analysis.

A-C Cleavage of recombinant MBP-GRI$^{25-168}$ fusion protein by recombinant AtMC9, followed by trypsin treatment and LC-MS/MS analyses using a Thermo LTQ Orbitrap XL mass spectrometer.

A Coomassie stain of representative samples on a 12% SDS-PAGE. (*) After 90 min incubation at 30˚C, a clear lower molecular weight band of MBP-GRI$^{25-168}$ was visible after proteolysis by AtMC9.

B After AtMC9 treatment, cleavage products of MBP-GRI$^{25-168}$ were N-terminally labeled in solution with trideutero- acetyl (<AcD3>). The annotated spectra covering the neo N-terminal peptides NH2<AcD3>-68LLVSHYK74 (Mascot score 60; Identity treshold score 33) and NH2<AcD3>-98GTSLLHCCKK107 (Mascot score 47; Identity treshold score 32) are shown.

C Position of the AtMC9 cleavage sites (↓) in the GRI$^{25-168}$ amino acid sequence. The identified <AcD3>-labelled peptides are underlined. Peptide coverage of the protein (93,7%) is represented in bold. Spectra of the <AcD3>-labeled peptides were visualized by Peptizer (Helsens *et al*., 2008).

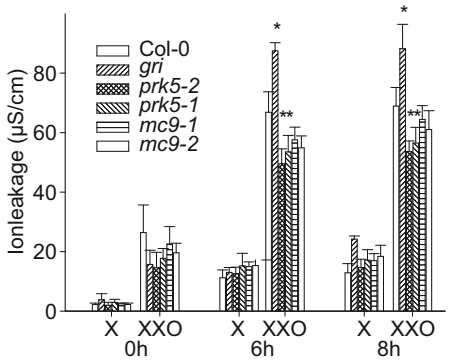

Fig. S14. Xanthine/xanthine oxidase infiltration of Col-0, *gri*, *prk5* and *atmc9* plants.

Enzymatic superoxide production from xanthine/xanthine oxidase (XXO) infiltration into Col-0, *prk5-1, prk5-2*, *atmc9-1*, *atmc9-2* and *gri* leaves (±SD of 4 replicates consisting of 4 leaf disks each). X is buffer control containing xanthine without xanthine oxidase.

Data information: Asterisks mark statistically significant differences from infiltration with GST according to Sidak's test ($P<0.05$). The experiment was repeated three times with similar results.

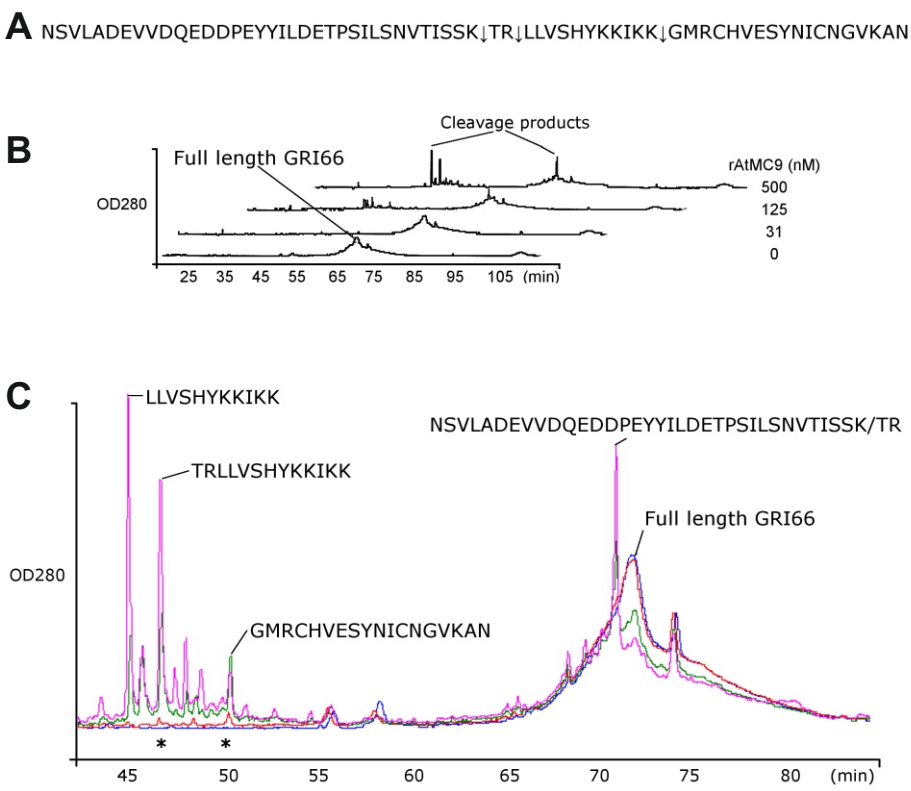

Fig. S15. GRI is cleaved by AtMC9 after K65, R67, K78 and K97, as revealed by *in vitro* cleavage assays and mass spectrometry analysis.

A-C Cleavage of biochemically pure GRIp$^{31\text{-}96}$ peptide (66 AA) by recombinant AtMC9, followed by immediate separation of cleavage products by reverse-phase chromatography (RP-HPLC) and size analysis by MALDI-TOF MS (Ultraflex, Bruker).

A GRIp$^{31\text{-}96}$ peptide was incubated with increasing concentrations of recombinant AtMC9 (rAtMC9) and cleavage products were separated on a C18 reverse-phase column. Cleavage sites in the GRIp$^{31\text{-}96}$ sequence are indicated with (↓). The experiment was performed twice with similar results.

B 3D view of the RP-HPLC UV absorbance chromatograms corresponding to the four concentrations of rAtMC9 used (as indicated in the figure).

C Overlapping view of the four RP-HPLC UV absorbance chromatograms indicating the peptide sequence of the main cleavage products (peptide mass was deduced by MALDI-TOF MS). The blue trace corresponds to 0 nM rAtMC9 sample, red trace to 31 nM rAtMC9 sample, green trace to 125 nM rAtMC9 sample and pink trace to 500 nM rAtMC9 sample. The first cleavage products to appear (highest in red trace and green trace) are indicated with asterisks. The mass of the full length GRIp$^{31\text{-}96}$ peptide was deduced by LC-MS/MS using a Thermo LTQ Orbitrap XL mass spectrometer, because it was not possible to deduce the mass by MALDI-TOF MS. The slash (/) in NSVLADEVVDQEDDPEYYILDETPSILS NVTISSK/TR indicates that both the longer (cleavage after R) and shorter (cleavage after K) cleavage products were present in the peak.

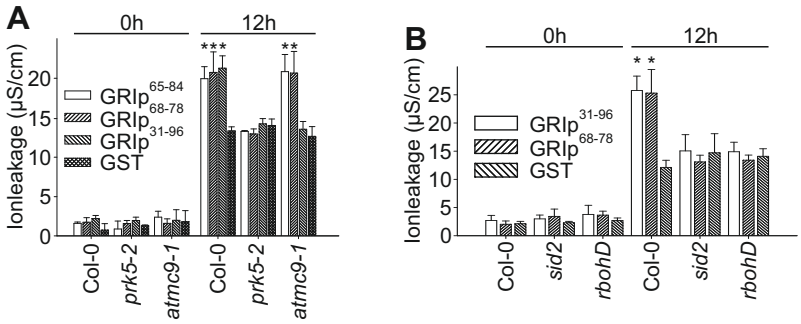

Fig. S16. Cell death by GRI-peptides is dependent on salicylic acid production and extracellular superoxide production.

A Infiltration of wild type, *prk5-2* and *atmc9-1* leaves with GRIp$^{31-96}$, GRIp$^{65-84}$, GRIp$^{68-78}$ or GST. GRIp$^{65-84}$ and GRIp$^{68-78}$ but not GRIp$^{31-96}$ were able to induce elevated ion leakage in the *atmc9-1* mutant (±SD of 4 replicates of 4 leaf disks each).

B Infiltration of wild type, *sid2* and *rbohD* leaves with 66 aa-long GRIp$^{31-96}$, 11 aa-long GRIp$^{68-78}$ or GST. GRIp$^{31-96}$ and GRIp$^{68-78}$ were able to induce elevated ion leakage in Col-0 but not in the mutants *sid2* and *rbohD* (±SD of 4 replicates of 4 leaf disks each).

Data information: Asterisks mark statistically significant differences from infiltration with GST according to Sidak's test ($P<0.05$). The experiments were repeated three times with similar results.

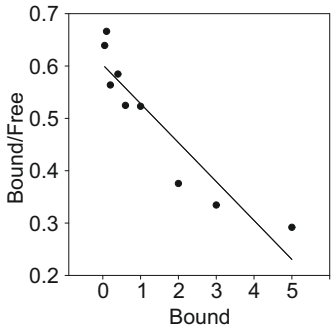

Fig. S17. Scatchard plot from data in Fig. 4G.

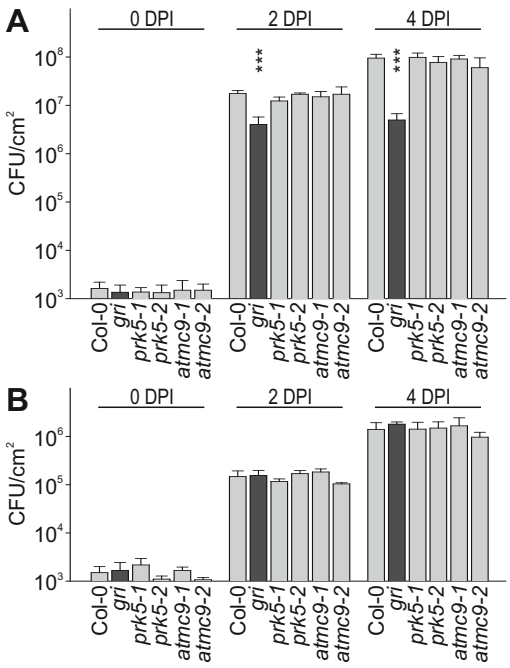

Fig. S18. Pathogen susceptibility in *gri*, *prk5* and *atmc9* plants.

4-week old plants were hand-infiltrated with 10^5 CFU/ml of *Pseudomonas syringae pv. tomato* (*Pto*) DC3000 (**A**) or DC3000 avrB (**B**), respectively. Subsequently, 4 leaf disks (total area 1 cm^2) were homogenized in 10 mM $MgCl_2$ and the bacterial count was determined by dilution plating one hour, two days and four days after infiltration.

Data information: Bars represent mean and error bars represent standard deviation of 3 replicates of 4 leaf disks each. Asterisks mark statistically significant differences from bacterial growth in Col-0 according to two-way anova with Tukey's HSD post-hoc test (P<0.001). For **A** bacterial growth in all lines is significantly different after two days from zero days, and for Col-0, *prk5-1*, *prk5-2*, *atmc9-1* and *atmc9-2* different at four days from two days post-infection. For **B** bacterial growth in all lines is significantly different after two days from zero days, and after four days from two days post-infection. All experiments were repeated three times with similar results.

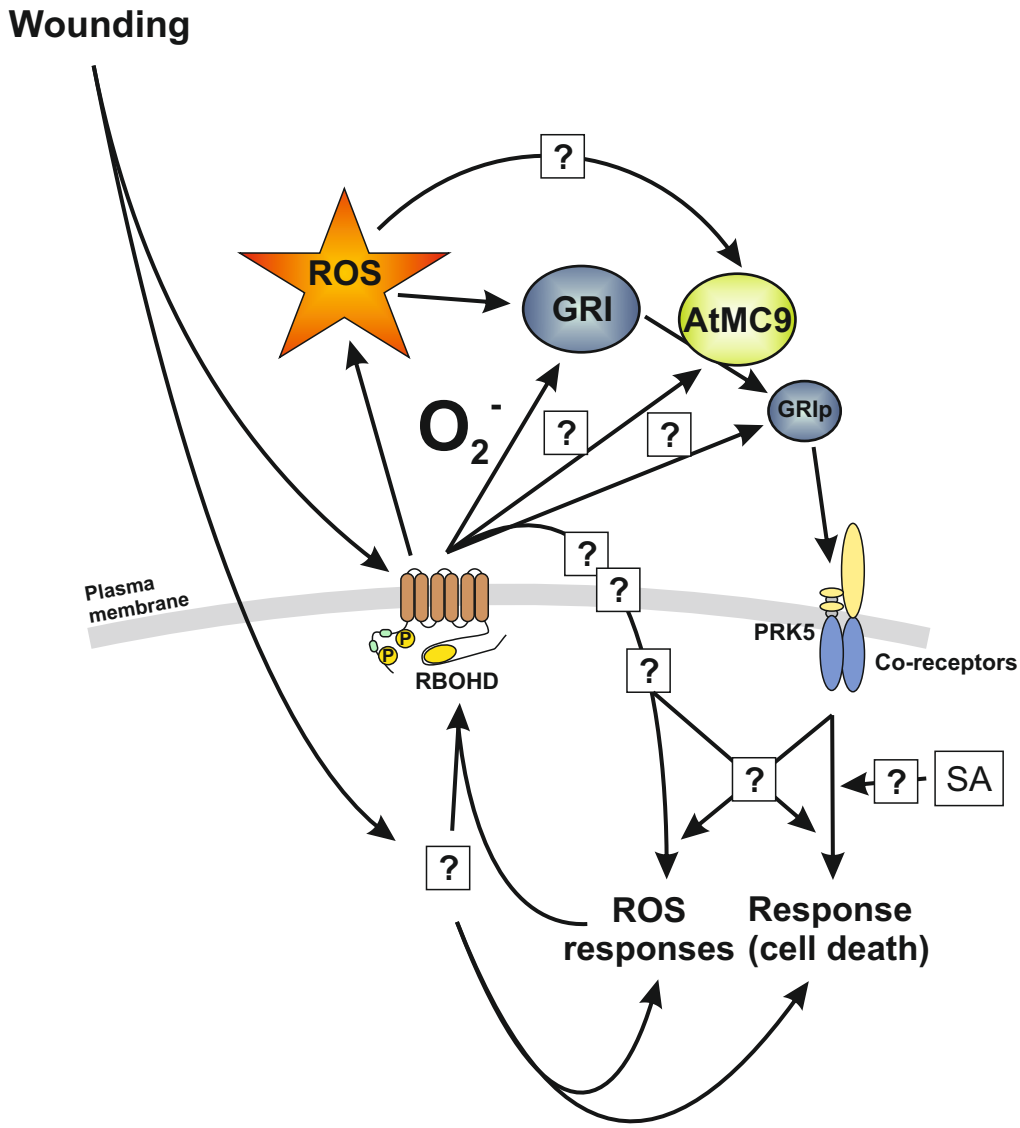

Fig. S19. Model of GRI function in ROS-induced cell death regulation.

Stress (for example wounding through peptide infiltration with a blunt syringe) leads to reactive oxygen species (ROS) production in the extracellular space by the NADPH oxidase RBOHD (producing superoxide, O_2^-). The secreted GRI protein is cleaved by AtMC9 and the resulting peptide (GRIp) is subsequently perceived by the enzymatically inactive RLK PRK5. It is currently unclear at what level ROS signalling interacts with GRI processing and perception. Alternatively signalling through ROS and GRI could represent parallel pathways which are only integrated at the intracellular response level. Salicylic acid (SA) is required for cell death induced by GRIp infiltration but the details of this interaction are currently not known. Co-receptors that are required for PRK5 action are hypothetical.